Journal of Power Sources 242 (2013) 683–686

Contents lists available at SciVerse ScienceDirect

Journal of Power Sources

journal homepage: www.elsevier.com/locate/jpowsour

Short communication

Micro-fibrous organic radical electrode to improve the electrochemical properties of organic rechargeable batteries

Jae-Kwang Kim*

Department of Applied Physics, Chalmers University of Technology, 412 96 Göteborg, Sweden

HIGHLIGHTS

- A micro-fibrous organic electrode film (MPE) has been prepared by electrospinning.
- The MPE based lithium cell displays a high discharge capacity of 111 mAh g^{-1} at 1C.
- The MPE has remarkably improved the volumetric capacity as 209 mAh cm^{-3} at 10C.

GRAPHICAL ABSTRACT

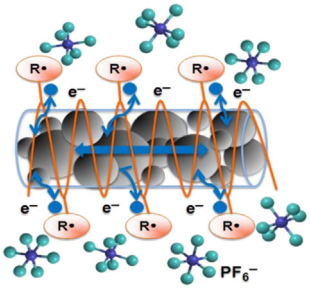

ARTICLE INFO

Article history:
Received 15 March 2013
Received in revised form
1 May 2013
Accepted 28 May 2013
Available online 10 June 2013

Keywords:
Micro-fibrous PTMA
Electrospinning
Volumetric capacity
Rate-capability
Organic rechargeable battery

ABSTRACT

A micro-fibrous organic electrode has been prepared by electrospinning process using poly(2,2,6,6-tetramethylpiperidinyloxy-4-ylmethacrylate) (PTMA), poly(vinylidene fluoride-co-hexafluoropropylene) (P(VdF-HFP)) and carbon black powder. The micro-fibrous PTMA electrode (MPE) film is investigated by FT-IR, TGA, SEM, TEM and electrochemical tests. The MPE shows excellent rate-capability and cycle performance. The MPE based lithium cell displays a high discharge capacity of 111 mAh g^{-1} at 1C. Even at a high current density of 50C, the MPE cell presents a discharge capacity of 109 mAh g^{-1}. Moreover, the MPE have remarkably improved the volumetric capacity (209 mAh cm^{-3} at 10C) compared with a nano-fibrous PTMA electrode. The excellent electrochemical performance is ascribed to the microstructure that promotes fast ion transport through short diffusion pathways and at the same time facilitates electron transport.

1. Introduction

Organic rechargeable batteries (ORBs) have been on the rise in recent years driven by their potential applications in flexible electronic devices. Beside the flexibility, the ORB is beneficial in terms of easy recycling/disposal, being environmentally friendly, utilizing unlimited material sources, being lightweight, and offering a high power density. Also, the energy density could be dramatically increased by design of the molecular structure. An early attempt to develop ORB used conducting polymers such as poly(acetylene) (PAC), polypyrrole (PPY) and polyaniline (PANI), but these batteries generally showed low capacity and poor cycleability [1,2]. Recently, carbonyl, sulfuric, organic crystal, and 2,2,6,6-tetramethylpiperi dinyloxy (TEMPO)-based organic materials have attracted attention as cathode for ORB [3–15].

Among the above materials, poly(2,2,6,6-tetramethylpiper idinyloxy-4-ylmethacrylate) (PTMA) containing the TEMPO radical is known to show redox behavior at 3.6 V vs. Li/Li+, at low

* Tel.: +46 31 772 3352; fax: +46 31 772 2090.
E-mail address: jaekwang@chalmers.se.

0378-7753/$ – see front matter © 2013 Elsevier B.V. All rights reserved.
http://dx.doi.org/10.1016/j.jpowsour.2013.05.169

rates. It also provides high power and rate capability with a theoretical cathode capacity of 111 mAh g^{-1}, due to a fast electron transfer rate [12]. However, a large amount carbon conductor has been necessary in the electrode, because PTMA is an insulator. Moreover, a poor contact with carbon conductor has been observed at high amounts of active material; with PTMA being dissolved into organic electrolytes and inducing self-discharge [16–18]. To improve the rate capability at high contents of active material graphene and CNT composite PTMA electrodes have been prepared, but cannot prevent the dissolution of active material [19,20]. Some strategies, such as using crosslinking, brush framework, mesocellular carbon, and ionic liquid etc [18,21–23], have been reported in order to dissolve the dissolution problem of PTMA.

We have also proposed a new strategy, a nano-fibrous PTMA film fabricated by electrospinning, to overcome the above-mentioned negative features of PTMA [24]. Although the nanofibrous morphology film has extraordinary rate capability, excellent cycleability, enhanced flexibility, and prevents dissolution, the nanostructure decrease the tap density and result in low volumetric energy density that needs to be considered in fabricating conventional batteries in industry.

Therefore, in this study, a micro-sized PTMA fibrous electrode film (hereafter MPE) is prepared to increase the volumetric capacity at high PTMA loadings ($\sim$9.0 mg cm^{-2}). The MPE shows improved volumetric capacity with excellent rate capability.

2. Experimental

PTMA was synthesized by the radical polymerization method as described in a previous study [16,18]. 2,2,6,6-Tetramethylpiperidine methacrylate monomer was polymerized by first using 2,2′-azobisisobutyronitrile radical initiator and then oxidizing with H_2O_2 in the presence of a $NaWO_4$ catalyst to obtain PTMA. 60 wt.% PTMA, 10 wt.% poly(vinylidene fluoride-co-hexafluoropropylene) (P(VdF-HFP)), and 30 wt.% carbon black powder were added to acetone and N-methylpyrrolidinone (1:1, w/w) solution. Electrospinning was performed by applying a voltage of 20 kV at room temperature. The electrospun micro-sized PTMA fibers were collected on an aluminum current collector to form an electrode film and vacuum dried at 80 °C for 12 h before further use [24]. An MPE based ORB was fabricated by stacking a lithium metal (300 μm thickness, Cyprus Foote Mineral Co.) anode with a Celgard 2200 separator film, and 1 M $LiPF_6$ in ethylene carbonate (EC)/dimethyl carbonate (DMC) (1:1 v/v) (Supplied from Samsung Co.) as the electrolyte. Electrochemical performance tests were carried out using an automatic galvanostatic charge–discharge unit, WBCS3000 battery cycler, between 3.0 and 4.0 V at room temperature, at various current densities. The size distribution of MPE was observed by transmission electron microscopy (TEM) performed on a JEM-2010 JEOL and scanning electron microscopy (SEM) using Philips XL30 S FEG. FT-IR absorption spectra were recorded with a Fourier transform interferometer (VERTEX 80v, Bruker Optics). The thermal stability was analyzed by thermogravimetric analysis (TGA) (SDT Q600 TA) in a nitrogen atmosphere at a heating rate of 10 °C min^{-1} from 20 °C to 800 °C.

3. Results and discussion

FT-IR spectra of PTMA, PVdF-HFP, and MPE are presented in Fig. 1. The main characteristic peaks of PVdF-HFP were assigned as follows, 1400, 1200 and 480 cm^{-1} attribute to CF_2 bending, CF_2 stretching, and CF_2 wagging [25]. The spectrum of PTMA shows absorption at 1728 and 1360 cm^{-1}, which corresponds to C=O and NO•. The spectrum of MPE has the characteristic peaks of both PTMA and PVdF-HFP, and broad peaks are displayed by addition of carbon. The peaks of MPE are almost the same with the precursors because of the absence of interactions between precursors.

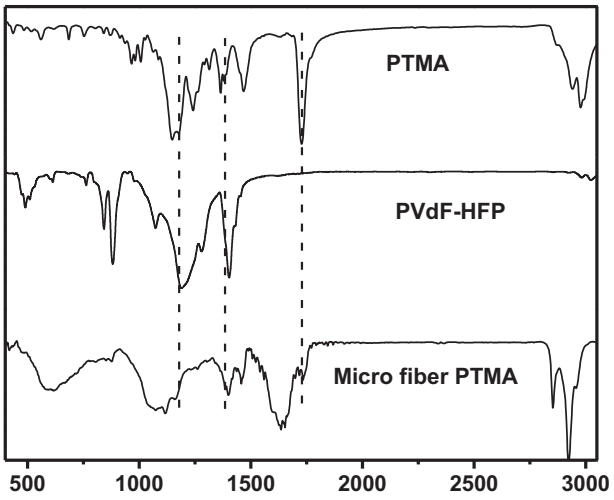

Fig. 1. FT-IR spectrum of PTMA, PVdF-HFP and micro-fiber PTMA electrode film.

The good thermal stability of MPE is revealed by TGA analysis of Fig. 2. An initial decomposition of PTMA occurs at 270 °C and 52 wt.% of PTMA in MPE is disappeared at 430 °C [26]. The initial decomposition of PVdF-HFP occurs at 430 °C and the decomposition of PVdF-HFP is completed at 500 °C with 8 wt.% loss. The dried carbon of 30 wt.% is maintained to 500 °C, and $\sim$10 wt.% ash from PTMA and PVdF-HFP is formed at 500 °C.

In Fig. 3a SEM image of MPE shows an interconnected network of long and continuous micro fibres with a diameter distribution from 1 μm to 5 μm. The high magnification of the inserted figure reveals the thick portion at the fiber caused by aggregation of carbon powder. The TEM image of Fig. 3b exhibits that the carbon black phase of the fiber is located mainly in the center of the organic fibers, although some aggregation of carbon black particles occur. The polymer layer on carbon black has a diameter distribution from 0.5 μm to 1 μm.

A simplified schematic of the micro organic fiber is given in Fig. 4a. The fully interconnected micron-sized pores in the film are filled with electrolyte. The nitroxyl radical of TEMPO is oxidized to form a cation and joins a PF_6^- of the electrolyte to form an

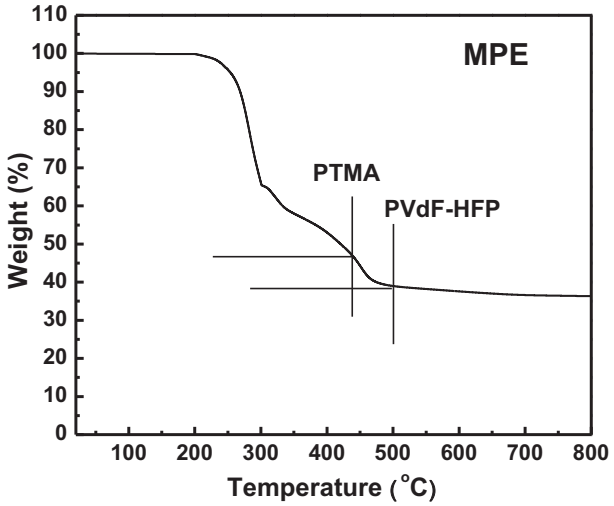

Fig. 2. TGA curve of micro-fibrous PTMA electrode film (MPE).

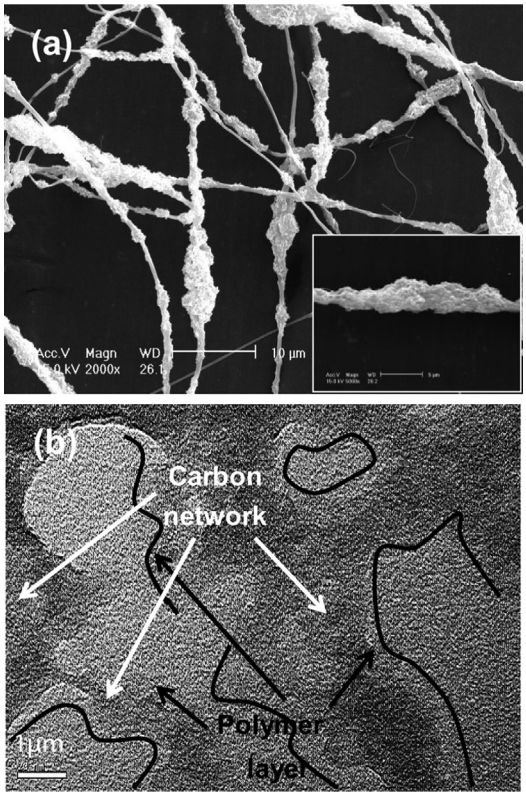

Fig. 3. SEM (a) and TEM (b) images of micro-fibrous PTMA.

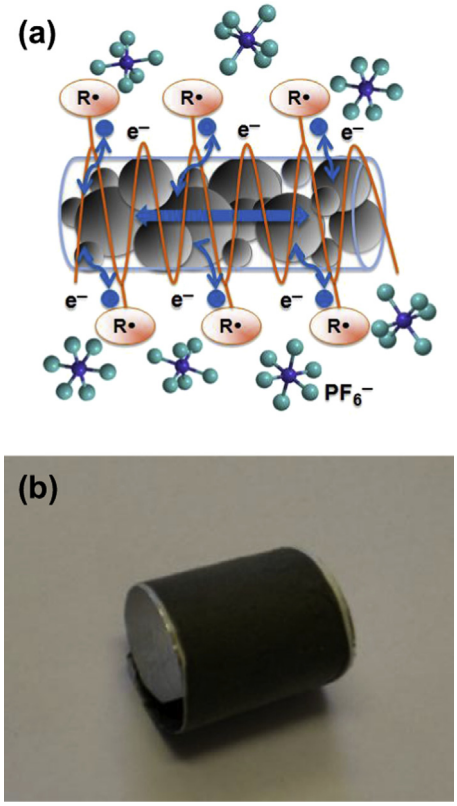

Fig. 4. Structure and mechanism (a) of micro-fibrous PTMA electrode (MPE), and photograph (b) of rolled-up state MPE.

oxoammonium salt during the anodic stage. During the cathodic stage the reverse reaction occurs. The external electron transfer through the polymer layer is apparently delivered by the self-exchange between neighboring nitroxyl radicals [27]. The electrons from the nitroxyl radical are delivered to the inner carbon network and the electron transfer is accelerated by the homogeneous carbon network [24]. Fig. 4b displays the MPE in a rolled-up state. The MPE shows high flexibility and sufficient mechanical strength for its use as a flexible organic electrode.

The initial discharge capacities of lithium cells, with an MPE of 45 μm thickness (without Al substrate), evaluated at 1C and 10C, are compared in Fig. 5a. With increasing current density, the discharge voltage shows a slight decreasing trend and the difference between charge and discharge voltages (ΔV) shows a small increase with C-rate, for 0.01 V at 1C-rate to 0.09 V at 10C-rate. Even at the high current density of 10C, a discharge capacity of 109.4 mAh g^{-1} is obtained, which is 99% of the theoretical capacity. These discharge capacities are higher than those reported in earlier studies employing liquid electrolytes and a 10 wt.% PTMA cathode [12,13] or a 50 wt.% PTMA cathode [28,29]. Moreover, the sudden capacity drop using 60 wt.% PTMA in the electrode does not occur for the MPE lithium cell [17]. From the charge–discharge profiles it is also seen that the Columbic efficiency of the first cycles were 100%, and that the battery showed excellent energy efficiency, >99%, at both current densities. The rate-capability and cycle performance of MPE at different current densities from 1 to 50C (Fig. 5b) reveal that MPE

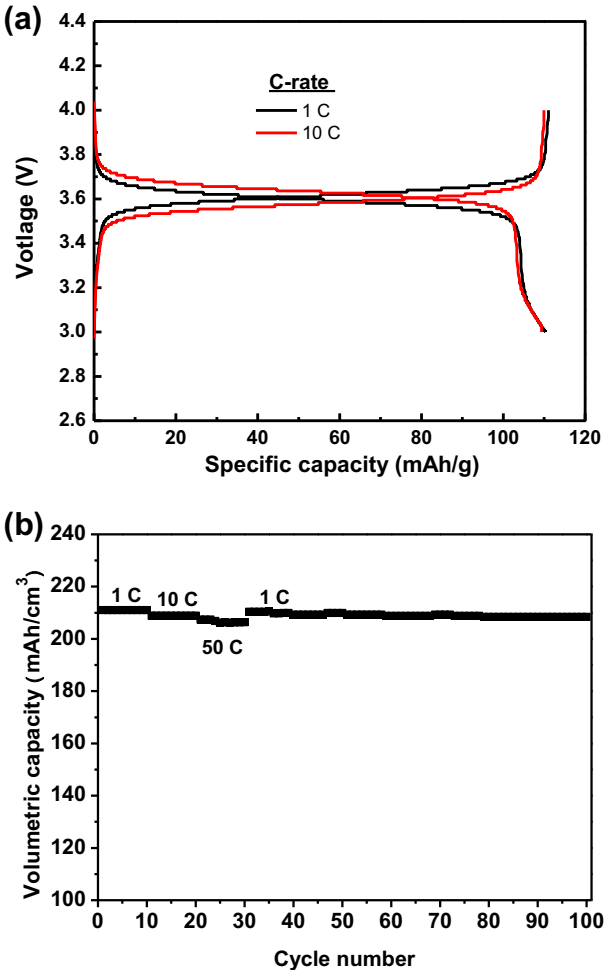

Fig. 5. Charge–discharge curves (a) and cycle performance (b) of micro-fibrous PTMA electrode film (MPE) at different current densities.

exhibits excellent rate-capability and cycle performance in the voltage range 3.0–4.0 V. The volumetric capacities based on the electrode density were 211, 209, and 207 mAh cm^{-3} at 1, 10, and 50C, respectively. The values are significantly improved compared with the nano-fibrous PTMA electrode and is close to inorganic electrodes at high current densities [24]. The capacity retention at 1C is close to 100% after 10 cycles. Even at the high current density of 50C, the capacity retention is as high as 99% and the MPE lithium cell maintains a discharge capacity of 108.6 mAh g^{-1} after 10 cycles.

The outstanding electrochemical properties of MPE are attributed to the particular morphology and structure of MPE, where the dispersive carbon black and PTMA active materials form a microfiber organic electrode film with micro pores and a large surface. The morphology and structure of MPE provide short ion diffusion lengths, offer high electronic conductivity and facilitate charge transfer within the electrode via the internal carbon network.

4. Conclusions

A micro-fibrous PTMA electrode film (MPE) is prepared by electrospinning process. This MPE exhibits excellent high rate-capability and cyclic stability in the voltage range 3.0–4.0 V. Furthermore, the volumetric capacity is significantly enhanced with high loading of PTMA. The excellent electrochemical performance is ascribed to the microstructure that promotes fast ion diffusion through short pathways and facilitates electron transport via the carbon network inside of the microfiber. In addition, the fibrous form of the film is beneficial to prepare a flexible electrode with sufficient mechanical strength.

Acknowledgments

The present work was supported by the Chalmers Area of Advance – Energy. I am thankful to Dr. Johan for his help to improve this paper.

References

[1] P. Novák, K. Müller, K.S.V. Santhanam, O. Haas, Chem. Rev. 97 (1997) 207.
[2] C.K. Jeong, J.H. Jung, B.H. Kim, S.Y. Lee, D.E. Lee, S.H. Jang, K.S. Ryu, J. Joo, Synth. Metals 117 (2001) 99.
[3] M. Armand, S. Grugeon, H. Vezin, S. Laruelle, P. Ribière, P. Poizot, J.-M. Tarascon, Nat. Mater. 8 (2009) 120.
[4] X. Han, C. Chang, L. Yuan, T. Sun, J. Sun, Adv. Mater. 19 (2007) 1616.
[5] Z. Song, H. Zhan, Y. Zhou, Angew. Chem. Int. Ed. 49 (2010) 8444.
[6] K. Pirnat, R. Dominko, R. Cerc-Korosec, G. Mali, B. Genorio, J. Power Sources 199 (2012) 308.
[7] M. Yao, H. Senoh, T. Sakai, T. Kiyobayashi, J. Power Sources 202 (2012) 364.
[8] D.J. Kim, S.H. Je, S. Sampath, J.W. Choi, A. Coskun, RSC Adv. 2 (2012) 7968.
[9] Y. Hanyu, Y. Ganbe, I. Honma, J. Power Sources 221 (2013) 186.
[10] J.T. Kearns, M.E. Roberts, J. Mater. Chem. 22 (2012) 2392.
[11] J.-K. Kim, F. Thébault, M.-Y. Heo, D.-S. Kim, Ö. Hansson, J.-H. Ahn, P. Johansson, L. Öhrström, A. Matic, P. Jacobsson, Electrochem. Commun. 21 (2012) 50.
[12] K. Nakahara, S. Iwasa, M. Satoh, Y. Morioka, J. Iriyama, M. Suguro, E. Hasegawa, Chem. Phys. Lett. 359 (2002) 351.
[13] H. Nishide, S. Iwasa, Y.-J. Pu, T. Suga, K. Nakahara, M. Satoh, Electrochim. Acta 50 (2004) 827.
[14] J.-K. Kim, G. Cheruvally, J.-W. Choi, J.-H. Ahn, D.-S. Choi, C.-E. Song, J. Electrochem. Soc. 154 (2007) A839.
[15] J.-K. Kim, A. Matic, J.-H. Ahn, P. Jacobsson, RSC Adv. 2 (2012) 10394.
[16] J.-K. Kim, G. Cheruvally, J.-W. Choi, J.-H. Ahn, S.-H. Lee, D.-S. Choi, C.-E. Song, Solid State Ionics 178 (2007) 1546.
[17] J.-K. Kim, G. Cheruvally, J.-H. Ahn, Y.-G. Seo, D.-S. Choi, S.-H. Lee, C.-E. Song, J. Ind. Eng. Chem. 14 (2008) 371.
[18] J.-K. Kim, A. Matic, J.-H. Ahn, P. Jacobsson, RSC Adv. 2 (2012) 9795.
[19] W. Guo, Y.X. Yin, S. Xin, Y.G. Guo, L.-J. Wan, Energy Environ. Sci. 5 (2012) 5221.
[20] W. Choi, S. Ohtani, K. Oyaizu, H. Nishide, K. Geckeler, Adv. Mater. 23 (2011) 4440.
[21] T. Suga, H. Konishi, H. Nishide, Chem. Commun. (2007) 1730.
[22] M.-K. Hung, Y.-H. Wang, C.-H. Lin, H.-C. Lin, J.-T. Lee, J. Mater. Chem. 22 (2012) 1570.
[23] Y. Kim, C. Jo, J. Lee, C.W. Lee, S. Yoon, J. Mater. Chem. 22 (2012) 1453.
[24] J.-K. Kim, J. Scheers, J.-H. Ahn, P. Johansson, A. Matic, P. Jacobsson, J. Mater. Chem. A 1 (2013) 2426.
[25] A.I. Gopalan, P. Santhosh, K.M. Manesh, J.H. Nho, S.H. Kim, C.-G. Hwang, K.-P. Lee, J. Membr. Sci. 325 (2008) 683.
[26] J.-K. Kim, J.-H. Ahn, G. Cheruvally, G.S. Chauhan, J.-W. Choi, D.-S. Kim, H.-J. Ahn, S.-H. Lee, C.-E. Song, Metall. Mater. Int. 15 (2009) 77.
[27] K. Nakahara, K. Oyaizu, H. Nishide, Chem. Lett. 40 (2011) 222.
[28] K. Nakahara, J. Iriyama, S. Iwasa, M. Suguro, M. Satoh, E.J. Cairns, J. Power Sources 163 (2007) 1110.
[29] K. Nakahara, J. Iriyama, S. Iwasa, M. Suguro, M. Satoh, E.J. Cairns, J. Power Sources 165 (2007) 398.